

Free vibration analysis of continuous bridge under the vehicles

Guojin Tan^a, Wensheng Wang, Yubo Jiao* and Zhigang Wei

College of Transportation, Jilin University, Renmin Street 5988, Changchun 130022, China

(Received June 29, 2016, Revised October 13, 2016, Accepted October 28, 2016)

Abstract. Free vibration analysis for continuous bridge under any number of vehicles is conducted in this paper. Calculation strategy for natural frequency and mode shape is proposed based on Euler-Bernoulli beam theory and numerical assembly method. Firstly, a half-car planar model is adopted; equations of motion and displacement functions for bridge and vehicle are established, respectively. Secondly, the undermined coefficient matrices for wheels, vehicles, intermediate support, left-end support and right-end support are derived. Then, the numerical assembly technique for conventional finite element method is adopted to construct the overall matrix of coefficients for whole system. Finally, natural frequencies and corresponding mode shapes are determined based on iterative method and overall matrix solution. Numerical simulation is presented to verify the effectiveness of the proposed method. The results reveal that the solutions of present method are exact ones. Natural frequencies and associate modal shapes of continuous bridge under different conditions of vehicles are investigated. The influences of vehicle parameters on natural frequencies are also demonstrated.

Keywords: continuous bridge; bridge-vehicle interaction; free vibration; numerical assembly method; numerical simulation

1. Introduction

It's known that while the physical properties are changed and the dynamic characteristics including modal frequencies and shapes will be changed (Wang and Qiao 2007). The dynamic characteristics of bridge structures have been widely applied to structural damage identification and condition assessment so far (O'Brien *et al.* 2015). In general, the existing methods for estimating dynamic characteristics fall into two general categories: 1) measured-input tests; and 2) ambient tests. The ambient excitation such as wind, traffic, microseism and so on is convenient and inexpensive. Wind-induced excitation is suitable for a broad band frequency and it could lead to a small amplitude of vibration. The level of vibration is too small to get satisfactory results especially for short span bridges. However, traffic-induced excitation has good effects for the measured dynamic characteristics and has been noted in numerous studies. The present author (Tan *et al.* 2011) thought that there is a large difference between the bridge loaded frequencies and natural frequencies under the vehicle. Biggs and Suer (1956) point out that the natural frequencies could vary as much as 20% while the test vehicle is on the bridge. Kim *et al.* (2003) investigated the Nongro simply supported bridge and found that the natural frequencies under light vehicles are up to 5.4% higher than those by heavy vehicles. Thus, it's of great importance to study the dynamic characteristics analysis of bridges under

the vehicles and the influence of vehicles on the dynamic characteristics of bridges.

The research on bridge-vehicle interaction has been conducted for decades, which can be back to the research of a pulsating load passing over a beam and the train crossing a bridge by Willis (1849), Stokes (1849) in the mid-19th century. In present researches, bridges are generally modelled as elastic beams, while the models for vehicles can be divided into three categories (Kim *et al.* 2005): the so-called moving load (Kumar *et al.* 2015, Gao *et al.* 2015), moving mass (Karimi and Ziaei-Rad 2015, Rieker and Trethewey 1999) and moving sprung-mass models (Liu and Du 2005, Yang and Yau 1997). The moving load model is the simplest one, which can obtain the dynamic properties of bridge with favorable accuracy. However, moving load model cannot consider the interaction between bridge and moving vehicles. For moving mass model, it takes into account of the inertia of vehicle, which is superior to moving load one. Nevertheless, it cannot assess the bouncing action of moving vehicle relative to bridge. Therefore, the sprung-mass model is proposed in order to overcome the drawbacks of moving load and moving mass models. It can realize the dynamic interaction between vehicles and bridge, which is close to the real conditions (Yang and Lin 2005). Azimi *et al.* (2013) investigated the effect of vehicle experiencing longitudinal acceleration on vehicle-bridge interaction, and a numerical vehicle-bridge interaction element to solve this problem was proposed. Shirai (2008) presented a comprehensive numerical model for demonstrating the bridge-vehicle interaction and resultant perceptible vibration. Ahmari *et al.* (2015) derived the governing equations for vibration of line supported orthotropic thin plates under the effect of moving vehicles based on Hamilton principle, and the effect of foundation

*Corresponding author, Ph.D.

E-mail: jiaoyb@jlu.edu.cn

^aPh.D.

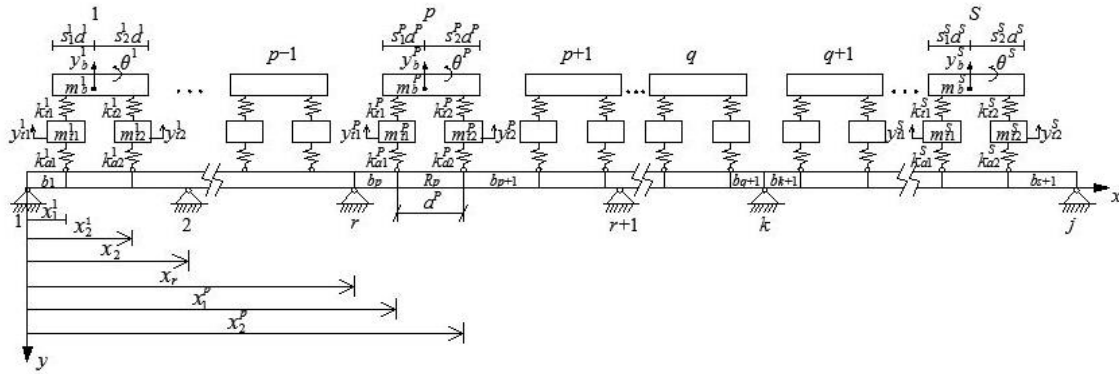


Fig. 1 Continuous bridge under multiple vehicles

settlement is considered. Yin *et al.* (2010) presented a novel approach for analyzing the non-stationary random response of bridge by using covariance equivalence technique, which could obtain more accurate bridge-vehicle interaction solutions. Zhu and Law (2002) investigated dynamic characteristics of multi-lane continuous bridge deck under the effect of moving vehicles with constant velocity. The dynamic properties of bridge deck were calculated using orthotropic plate theory and modal superposition technique.

From above literature review, a great majority of efforts are paid to the dynamic response of bridge-vehicle interaction in time domain, while the attention for dynamic properties of frequency contents is relatively limited. Yang and Lin (2005) studied the dynamic interaction between a moving vehicle and bridge, and the frequency aspects were especially demonstrated. Cha (2001) obtained the natural frequencies of linear structure under the effect of sprung-mass systems based on the assumed-modes method. Naguleswaran (2003) used a fourth-order determinant equated to zero, the frequencies of a Euler-Bernoulli beam with up to five elastic supports were calculated. Wu and Chou (1999) derived the exact solution of a uniform beam under any number of sprung-mass systems by use of numerical assembly method. Shi *et al.* (2014) made a semi-analytical method for solving the vibration equation of the non-uniform beam with added masses and elastic supports by extending the application of the modal perturbation method based on the Bernoulli-Euler beam theory. These researches have obtained the exact solutions for the natural frequencies and mode shapes of single-span bridges carrying sprung-mass systems. However, the exact solutions for the natural frequencies and mode shapes of multi-span bridges need to be investigated. Although Lin and Tsai (2007) proposed the exact solutions for the natural frequencies and mode shapes of a uniform multi-span beam carrying multiple sprung-mass systems, the sprung-mass model is relatively simple. A more complex and representative bridge-vehicle model for the dynamic interaction analysis need to be conducted.

In this paper, a calculation method for natural frequencies and mode shapes of multi-span bridge under any number of vehicles was proposed. The dynamic formulas for bridge-vehicle interaction were determined through displacement coordination equation and boundary conditions. Therefore, the natural frequencies and mode

shapes of bridge can be obtained by solving matrix eigenvalues.

2. Equation of motion and displacement function

The sketch for a uniform bridge with $(j-1)$ spans is shown in Fig. 1, which is under s vehicles. As can be seen from this figure, a half-car planar model is adopted to simulate the vehicles on the bridge. 1, ..., $p-1$, p , $p+1$, ..., q , $q+1$, ..., s are vehicle numbers; 1, 2, ..., r , $r+1$, ..., k , ..., j are pinned supports. This continuous bridge is divided into multiple sections by vehicles and supports. $b_1, \dots, b_p, R_p, b_{p+1}, \dots, b_{q+1}, b_{k+1}, \dots, b_{s+1}$ are section numbers; while $l_{b_1}, \dots, l_{b_p}, l_{R_p}, l_{b_{p+1}}, \dots, l_{b_{q+1}}, l_{b_{k+1}}, \dots, l_{b_{s+1}}$ are corresponding section lengths. $m_b^i, I_b^i, m_{t1}^i, m_{t2}^i$ ($i=1,2,\dots,s$) are sprung mass, rotatory mass and wheel masses for i th vehicle; while k_{t1}^i and k_{t2}^i are suspension spring constants, k_{a1}^i and k_{a2}^i are tyre stiffness coefficients, a^i is the distance between two wheels. For coordinates, the positions for pinned supports are defined by x_r ($r=2,\dots,j$), those for left wheels of half-car planar model are defined by x_1^p ($p=1,2,\dots,s$), and those for right wheels of half-car planar model are defined by x_2^p ($p=1,2,\dots,s$).

2.1 Equation of motion and displacement function for bridge

Assuming $\xi = x - x_1^p$, for section R_p , $x_1^p \leq x \leq x_2^p$. Therefore, $0 \leq \xi \leq l_{R_p}$. Equation of motion for section R_p can be established based on Euler-Bernoulli beam theory, which is given by Eq. (1)

$$EI \frac{\partial^4 y(\xi, t)}{\partial x^4} + m \frac{\partial^2 y(\xi, t)}{\partial t^2} = 0 \tag{1}$$

where EI and m are flexural rigidity and mass per unit length of section, respectively. E is elastic modulus, and I is moment of inertia. $y(\xi, t)$ is transverse deflection of R_p section at position ξ and time t .

Assuming the whole vibrating system shown in Fig. 1 performs harmonic free vibration at equilibrium position, it

has Eq. (2)

$$y(\xi, t) = \phi_{R_p}(\xi) \cdot e^{j\omega t} \quad (2)$$

where ω is natural frequency of the whole vibrating system, $\phi_{R_p}(\xi)$ is vibration mode function for R_p and amplitude of $y(\xi, t)$, $j = \sqrt{-1}$.

The substitution of Eq. (2) into Eq. (1) obtains Eq. (3)

$$\phi_{R_p}(\xi) = A_{R_p} \sin \beta \xi + B_{R_p} \cos \beta \xi + C_{R_p} \sinh \beta \xi + D_{R_p} \cosh \beta \xi \quad (3)$$

where $A_{R_p}, B_{R_p}, C_{R_p}, D_{R_p}$ are undetermined coefficients for section R_p , and $\beta^4 = \omega^2 m / EI$.

2.2 Equation of motion and displacement function for vehicle

Taking the p th vehicle for example, the equations of motion for wheel masses m_{t1}^p and m_{t2}^p are given by Eq. (4)

$$\left. \begin{aligned} m_{t1}^p \ddot{y}_{t1}^p + k_{a1}^p (y_{t1}^p + y_1^p) + k_{t1}^p (y_{t1}^p - y_b^p + s_1^p a^p \theta^p) &= 0 \\ m_{t2}^p \ddot{y}_{t2}^p + k_{a2}^p (y_{t2}^p + y_2^p) + k_{t2}^p (y_{t2}^p - y_b^p - s_2^p a^p \theta^p) &= 0 \end{aligned} \right\} \quad (4)$$

The force balance equations for vehicle body (sprung mass m_b^p , rotatory mass I_b^p) are Eq. (5)

$$\left. \begin{aligned} m_b^p \ddot{y}_b^p + k_{t1}^p (y_b^p - y_{t1}^p - s_1^p a^p \theta^p) + k_{t2}^p (y_b^p - y_{t2}^p + s_2^p a^p \theta^p) &= 0 \\ I_b^p \ddot{\theta}^p - s_1^p a^p k_{t1}^p (y_b^p - y_{t1}^p - s_1^p a^p \theta^p) + s_2^p a^p k_{t2}^p (y_b^p - y_{t2}^p + s_2^p a^p \theta^p) &= 0 \end{aligned} \right\} \quad (5)$$

where Eqs. (4)-(5) are the equilibrium equations of motion for vehicles. y_b^p is transverse displacement of vehicle body; θ^p is rotation angle for vehicle body; y_{t1}^p and y_{t2}^p are transverse displacements of left and right wheels of vehicle, respectively; $s_1^p a^p$ and $s_2^p a^p$ are distances from body's center of gravity to left wheel and right wheel of vehicle, respectively; y_1^p, y_2^p are deflections of beam at positions x_1^p and x_2^p , respectively.

Because the whole vibrating system performs harmonic free vibration, it can obtain Eq. (6)

$$\left. \begin{aligned} y_{t1}^p &= Y_{t1}^p e^{j\omega t} \\ y_{t2}^p &= Y_{t2}^p e^{j\omega t} \\ y_b^p &= Y_b^p e^{j\omega t} \\ \theta^p &= \hat{\theta}^p e^{j\omega t} \end{aligned} \right\} \quad (6)$$

where $Y_{t1}^p, Y_{t2}^p, Y_b^p$ and $\hat{\theta}^p$ are the amplitudes of $y_{t1}^p, y_{t2}^p, y_b^p$ and θ^p , respectively. They are undetermined coefficients for amplitudes.

3. Equations of undetermined coefficients

3.1 Equations at wheels

Shear force increment at left wheel of p th vehicle (x_1^p) between sections b_p and R_p can be calculated by $m_{t1} \ddot{y}_{t1} + k_{t1} (y_{t1} - y_b + s_1^p a^p \theta^p)$. It requires continuous rotation and displacement, equivalent bending moment and shear force at position x_1^p . Eq. (7) can be obtained based on Eqs. (2) and (6).

$$\left. \begin{aligned} \phi_{b_p}(l_{b_p}) &= \phi_{R_p}(0) \\ \phi_{b_p}'(l_{b_p}) &= \phi_{R_p}'(0) \\ \phi_{b_p}''(l_{b_p}) &= \phi_{R_p}''(0) \\ EI \phi_{b_p}'''(l_{b_p}) - \omega^2 m_{t1}^p Y_{t1}^p \\ + k_{t1}^p (Y_{t1}^p - Y_b^p + s_1^p a^p \hat{\theta}^p) &= EI \phi_{R_p}'''(0) \end{aligned} \right\} \quad (7)$$

where ϕ_{b_p} is modal function for section b_p .

The substitution of Eq. (3) into Eq. (7), one obtains Eqs.(8)-(11)

$$A_{b_p} \sin \beta l_{b_p} + B_{b_p} \cos \beta l_{b_p} + C_{b_p} \sinh \beta l_{b_p} + D_{b_p} \cosh \beta l_{b_p} - B_{R_p} - D_{R_p} = 0 \quad (8)$$

$$A_{b_p} \cos \beta l_{b_p} - B_{b_p} \sin \beta l_{b_p} + C_{b_p} \cosh \beta l_{b_p} + D_{b_p} \sinh \beta l_{b_p} - A_{R_p} - C_{R_p} = 0 \quad (9)$$

$$-A_{b_p} \sin \beta l_{b_p} - B_{b_p} \cos \beta l_{b_p} + C_{b_p} \sinh \beta l_{b_p} + D_{b_p} \cosh \beta l_{b_p} + B_{R_p} - D_{R_p} = 0 \quad (10)$$

$$EI \beta^3 (-A_{b_p} \cos \beta l_{b_p} + B_{b_p} \sin \beta l_{b_p} + C_{b_p} \cosh \beta l_{b_p} + D_{b_p} \sinh \beta l_{b_p}) - \omega^2 m_{t1}^p Y_{t1}^p + k_{t1}^p (Y_{t1}^p - Y_b^p + s_1^p a^p \hat{\theta}^p) + EI \beta^3 (A_{R_p} - C_{R_p}) = 0 \quad (11)$$

$A_{b_p}, B_{b_p}, C_{b_p}$ and D_{b_p} are undetermined coefficients for modal shape of section b_p .

Transforming Eqs. (8)-(11) into matrix form, one has Eq. (12)

$$[\mathbf{H}_{pl}] \{ \mathbf{U}_{pl} \} = [\mathbf{H}_{pl1} \quad \mathbf{H}_{pl2} \quad \mathbf{H}_{pl3}] \begin{Bmatrix} \mathbf{U}_{b_p} \\ \mathbf{U}_{R_p} \\ \mathbf{U}_{pv} \end{Bmatrix} = 0 \quad (12)$$

where

$$[\mathbf{H}_{pl1}] = \begin{bmatrix} n+1 & n+2 \\ \sin \beta l_{b_p} & \cos \beta l_{b_p} \\ \cos \beta l_{b_p} & -\sin \beta l_{b_p} \\ -\sin \beta l_{b_p} & -\cos \beta l_{b_p} \\ -EI \beta^3 \cos \beta l_{b_p} & EI \beta^3 \sin \beta l_{b_p} \end{bmatrix} \quad (13)$$

$$\begin{bmatrix} n+3 & n+4 \\ \sinh \beta l_{b_p} & \cosh \beta l_{b_p} \\ \cosh \beta l_{b_p} & \sinh \beta l_{b_p} \\ \sinh \beta l_{b_p} & \cosh \beta l_{b_p} \\ EI \beta^3 \cosh \beta l_{b_p} & EI \beta^3 \sinh \beta l_{b_p} \end{bmatrix} \begin{matrix} m+1 \\ m+2 \\ m+3 \\ m+4 \end{matrix}$$

$$[\mathbf{H}_{p12} \quad \mathbf{H}_{p13}] = \begin{bmatrix} n+5 & n+6 & n+7 & n+8 \\ 0 & -1 & 0 & -1 \\ -1 & 0 & -1 & 0 \\ 0 & 1 & 0 & -1 \\ EI\beta^3 & 0 & -EI\beta^3 & 0 \end{bmatrix} \quad (14)$$

$$\begin{bmatrix} n+9 & n+10 & n+11 & n+12 \\ 0 & 0 & 0 & 0 \\ 0 & 0 & 0 & 0 \\ 0 & 0 & 0 & 0 \\ -\omega^2 m_{t1}^p + k_{t1}^p & 0 & -k_{t1}^p & s_1^p a^p k_{t1}^p \end{bmatrix} \begin{matrix} m+1 \\ m+2 \\ m+3 \\ m+4 \end{matrix}$$

$$\left. \begin{matrix} \{\mathbf{U}_{b_p}\} = \{A_{b_p} \quad B_{b_p} \quad C_{b_p} \quad D_{b_p}\}^T \\ \{\mathbf{U}_{R_p}\} = \{A_{R_p} \quad B_{R_p} \quad C_{R_p} \quad D_{R_p}\}^T \\ \{\mathbf{U}_{pv}\} = \{Y_{t1} \quad Y_{t2} \quad Y_b \quad \hat{\theta}^p\}^T \end{matrix} \right\} \quad (15)$$

and

$$\left. \begin{matrix} m = 12(p-1) + 4(r-1) + 2 \\ n = 4\{2(p-1) + (r-1)\} \\ + 4(p-1) = 12(p-1) + 4(r-1) \end{matrix} \right\} \quad (16)$$

here p is vehicle number; r is pinned support number which is closest to x_1^p among 0 and x_1^p .

At the right wheel of the p th vehicle (wheel at x_2^p), it can also obtain Eqs. (17)-(21)

$$A_{R_p} \sin \beta l_{R_p} + B_{R_p} \cos \beta l_{R_p} + C_{R_p} \sinh \beta l_{R_p} + D_{R_p} \cosh \beta l_{R_p} - B_{b_{p+1}} - D_{b_{p+1}} = 0 \quad (17)$$

$$A_{R_p} \cos \beta l_{R_p} - B_{R_p} \sin \beta l_{R_p} + C_{R_p} \cosh \beta l_{R_p} + D_{R_p} \sinh \beta l_{R_p} - A_{b_{p+1}} - C_{b_{p+1}} = 0 \quad (18)$$

$$-A_{R_p} \sin \beta l_{R_p} - B_{R_p} \cos \beta l_{R_p} + C_{R_p} \sinh \beta l_{R_p} + D_{R_p} \cosh \beta l_{R_p} + B_{b_{p+1}} - D_{b_{p+1}} = 0 \quad (19)$$

$$EI\beta^3(-A_{R_p} \cos \beta l_{R_p} + B_{R_p} \sin \beta l_{R_p} + C_{R_p} \cosh \beta l_{R_p} + D_{R_p} \sinh \beta l_{R_p}) - \omega^2 m_{t2}^p Y_{t2}^p + k_{t2}^p (Y_{t2}^p - Y_b^p + s_2^p a^p \hat{\theta}^p) + EI\beta^3(A_{b_{p+1}} - C_{b_{p+1}}) = 0 \quad (20)$$

$$[\mathbf{H}_{pr}] \{\mathbf{U}_{pr}\} = [\mathbf{H}_{pr1} \quad \mathbf{H}_{pr2} \quad \mathbf{H}_{pr3}] \begin{Bmatrix} \mathbf{U}_{R_p} \\ \mathbf{U}_{pv} \\ \mathbf{U}_{b_{p+1}} \end{Bmatrix} = 0 \quad (21)$$

where

$$[\mathbf{H}_{pr1}] = \begin{bmatrix} n+5 & n+6 \\ \sin \beta l_{R_p} & \cos \beta l_{R_p} \\ \cos \beta l_{R_p} & -\sin \beta l_{R_p} \\ -\sin \beta l_{R_p} & -\cos \beta l_{R_p} \\ -EI\beta^3 \cos \beta l_{R_p} & EI\beta^3 \sin \beta l_{R_p} \end{bmatrix} \quad (22)$$

$$\begin{bmatrix} n+7 & n+8 \\ \sinh \beta l_{R_p} & \cosh \beta l_{R_p} \\ \cosh \beta l_{R_p} & \sinh \beta l_{R_p} \\ \sinh \beta l_{R_p} & \cosh \beta l_{R_p} \\ EI\beta^3 \cosh \beta l_{R_p} & EI\beta^3 \sinh \beta l_{R_p} \end{bmatrix} \begin{matrix} m+5 \\ m+6 \\ m+7 \\ m+8 \end{matrix}$$

$$[\mathbf{H}_{pr2} \quad \mathbf{H}_{pr3}] = \begin{bmatrix} n+9 & n+10 & n+11 \\ 0 & 0 & 0 \\ 0 & 0 & 0 \\ 0 & -\omega^2 m_{t2}^p + k_{t2}^p & -k_{t2}^p \end{bmatrix} \quad (23)$$

$$\begin{bmatrix} n+12 & n+13 & n+14 & n+15 & n+16 \\ 0 & 0 & -1 & 0 & -1 \\ 0 & -1 & 0 & -1 & 0 \\ 0 & 0 & 1 & 0 & -1 \\ -s_2^p a^p k_{t2}^p & EI\beta^3 & 0 & -EI\beta^3 & 0 \end{bmatrix} \begin{matrix} m+5 \\ m+6 \\ m+7 \\ m+8 \end{matrix}$$

$$\{\mathbf{U}_{b_{p+1}}\} = \{A_{b_{p+1}} \quad B_{b_{p+1}} \quad C_{b_{p+1}} \quad D_{b_{p+1}}\}^T \quad (24)$$

$A_{b_{p+1}}, B_{b_{p+1}}, C_{b_{p+1}}$ and $D_{b_{p+1}}$ are undetermined coefficients for section b_{p+1} .

3.2 Equations from motion of vehicles

The substitutions of Eqs. (2)-(3) and (6) into Eqs. (4)-(5), one obtains Eqs. (25)-(28)

$$k_{a1}^p (B_{R_p} + D_{R_p}) - \omega^2 m_{t1}^p Y_{t1}^p + k_{a1}^p Y_{t1}^p + k_{t1}^p (Y_{t1}^p - Y_b^p + s_1^p a^p \hat{\theta}^p) = 0 \quad (25)$$

$$k_{a2}^p (B_{b_{p+1}} + D_{b_{p+1}}) - \omega^2 m_{t2}^p Y_{t2}^p + k_{a1}^p Y_{t1}^p + k_{t2}^p (Y_{t2}^p - Y_b^p - s_2^p a^p \hat{\theta}^p) = 0 \quad (26)$$

$$-\omega^2 m_b^p Y_b^p + k_{t1}^p (Y_b^p - Y_{t1}^p - s_1^p a^p \hat{\theta}^p) + k_{t2}^p (Y_b^p - Y_{t2}^p + s_2^p a^p \hat{\theta}^p) = 0 \quad (27)$$

$$-\omega^2 I_b^p \hat{\theta}^p - s_1^p a^p k_{t1}^p (Y_b^p - Y_{t1}^p - s_1^p a^p \hat{\theta}^p) + s_2^p a^p k_{t2}^p (Y_b^p - Y_{t2}^p + s_2^p a^p \hat{\theta}^p) = 0 \quad (28)$$

or

$$[\mathbf{H}_v^p] \{\mathbf{U}_v^p\} = [\mathbf{H}_{v1}^p \quad \mathbf{H}_{v2}^p \quad \mathbf{H}_{v3}^p] \begin{Bmatrix} \mathbf{U}_{R_p} \\ \mathbf{U}_{pv} \\ \mathbf{U}_{b_{p+1}} \end{Bmatrix} = 0 \quad (29)$$

where

$$[\mathbf{H}_{v1}^p] = \begin{bmatrix} n+5 & n+6 & n+7 & n+8 \\ 0 & k_{a1}^p & 0 & k_{a1}^p \\ 0 & 0 & 0 & 0 \\ 0 & 0 & 0 & 0 \\ 0 & 0 & 0 & 0 \end{bmatrix} \begin{matrix} m+9 \\ m+10 \\ m+11 \\ m+12 \end{matrix} \quad (30)$$

$$\begin{aligned}
 \left[\mathbf{H}_{v2}^p \right] &= \begin{bmatrix} n+9 & n+10 \\ -\omega^2 m_{i1}^p + k_{a1}^p + k_{r1}^p & 0 \\ 0 & -\omega^2 m_{i2}^p + k_{a2}^p + k_{r2}^p \\ -k_{r1}^p & -k_{r2}^p \\ s_1^p a^p k_{r1}^p & -s_2^p a^p k_{r2}^p \end{bmatrix} \quad (31) \\
 \left[\mathbf{H}_{v3}^p \right] &= \begin{bmatrix} n+11 & n+12 \\ -k_{i1}^p & s_1^p a^p k_{i1}^p \\ -k_{i2}^p & -s_2^p a^p k_{i2}^p \\ -\omega^2 m_b^p + k_{i1}^p + k_{r2}^p & s_2^p a^p k_{i2}^p - s_1^p a^p k_{i1}^p \\ s_2^p a^p k_{i2}^p - s_1^p a^p k_{i1}^p & -\omega^2 I_b^p + (a^p)^2 \left((s_2^p)^2 k_{i2}^p + (s_1^p)^2 k_{i1}^p \right) \end{bmatrix} \begin{matrix} m+9 \\ m+10 \\ m+11 \\ m+12 \end{matrix} \\
 \left[\mathbf{H}_{v3}^p \right] &= \begin{bmatrix} n+13 & n+14 & n+15 & n+16 \\ 0 & 0 & 0 & 0 \\ 0 & k_{a2}^p & 0 & k_{a2}^p \\ 0 & 0 & 0 & 0 \\ 0 & 0 & 0 & 0 \end{bmatrix} \begin{matrix} m+9 \\ m+10 \\ m+11 \\ m+12 \end{matrix} \quad (32)
 \end{aligned}$$

3.3 Equations at intermediate pinned supports

From Fig. 1, middle pinned support r is between section b_{q+1} of $(k-1)$ th span and section b_{k+1} of k th span. Then, the displacement of right end at b_{q+1} section for the $(k-1)$ th span is zero, and the left end at the first section for k th span is zero. One has Eqs. (33)-(34)

$$\phi_{b_{k+1}}(0) = 0 \quad (33)$$

$$\phi_{b_{q+1}}(l_{q+1}) = 0 \quad (34)$$

According to continuous deformation and moment equilibrium at k th intermediate support, it can obtain that Eqs. (35)-(36)

$$\phi'_{b_{q+1}}(l_{b_{q+1}}) = \phi'_{b_{k+1}}(0) \quad (35)$$

$$\phi''_{b_{q+1}}(l_{b_{q+1}}) = \phi''_{b_{k+1}}(0) \quad (36)$$

The substitution of Eq. (3) into Eqs. (33)-(36), one obtains Eqs. (37)-(40)

$$\begin{aligned}
 A_{b_{q+1}} \sin \beta l_{b_{q+1}} + B_{b_{q+1}} \cos \beta l_{b_{q+1}} + C_{b_{q+1}} \sinh \beta l_{b_{q+1}} \\
 + D_{b_{q+1}} \cosh \beta l_{b_{q+1}} = 0 \quad (37)
 \end{aligned}$$

$$B_{b_{k+1}} + D_{b_{k+1}} = 0 \quad (38)$$

$$\begin{aligned}
 A_{b_{q+1}} \cos \beta l_{b_{q+1}} - B_{b_{q+1}} \sin \beta l_{b_{q+1}} + C_{b_{q+1}} \cosh \beta l_{b_{q+1}} + D_{b_{q+1}} \sinh \beta l_{b_{q+1}} \\
 - A_{b_{k+1}} - C_{b_{k+1}} = 0 \quad (39)
 \end{aligned}$$

$$\begin{aligned}
 -A_{b_{q+1}} \sin \beta l_{b_{q+1}} - B_{b_{q+1}} \cos \beta l_{b_{q+1}} + C_{b_{q+1}} \sinh \beta l_{b_{q+1}} + D_{b_{q+1}} \cosh \beta l_{b_{q+1}} \\
 + B_{b_{k+1}} - D_{b_{k+1}} = 0 \quad (40)
 \end{aligned}$$

where $A_{b_{q+1}}, B_{b_{q+1}}, C_{b_{q+1}}, D_{b_{q+1}}$ are undetermined coefficients for modal shape function of section b_{q+1} ; while $A_{b_{k+1}}, B_{b_{k+1}}, C_{b_{k+1}}, D_{b_{k+1}}$ are undetermined coefficients for section b_{k+1} .

Transforming Eqs. (37)-(40) into matrix form, one obtains Eq. (41)

$$\left[\mathbf{H}_s \right] \left\{ \mathbf{U}_s \right\} = 0 \quad (41)$$

where

$$\left[\mathbf{H}_s \right] = \begin{bmatrix} n'+1 & n'+2 & n'+3 \\ \sin \beta l_{b_{q+1}} & \cos \beta l_{b_{q+1}} & \sinh \beta l_{b_{q+1}} \\ 0 & 0 & 0 \\ \cos \beta l_{b_{q+1}} & -\sin \beta l_{b_{q+1}} & \cosh \beta l_{b_{q+1}} \\ -\sin \beta l_{b_{q+1}} & -\cos \beta l_{b_{q+1}} & \sinh \beta l_{b_{q+1}} \end{bmatrix} \quad (42)$$

$$\begin{bmatrix} n'+4 & n'+5 & n'+6 & n'+7 & n'+8 \\ \cosh \beta l_{b_{q+1}} & 0 & 0 & 0 & 0 \\ 0 & 0 & 1 & 0 & 1 \\ \sinh \beta l_{b_{q+1}} & -1 & 0 & -1 & 0 \\ \cosh \beta l_{b_{q+1}} & 0 & 1 & 0 & -1 \end{bmatrix} \begin{matrix} m'+1 \\ m'+2 \\ m'+3 \\ m'+4 \end{matrix}$$

$$\left\{ \mathbf{U}_s \right\} = \left\{ \begin{matrix} n'+1 & n'+2 & n'+3 & n'+4 \\ A_{b_{q+1}} & B_{b_{q+1}} & C_{b_{q+1}} & D_{b_{q+1}} \\ n'+5 & n'+6 & n'+7 & n'+8 \\ A_{b_{k+1}} & B_{b_{k+1}} & C_{b_{k+1}} & D_{b_{k+1}} \end{matrix} \right\}^T \quad (43)$$

and

$$\left. \begin{aligned} m' &= 12q + 4(k-2) + 2 \\ n' &= 4(2q + (k-2)) + 4q = 12q + 4(k-2) \end{aligned} \right\} \quad (44)$$

here k is number of intermediate support, q is vehicle number which is closest to x_k among 0 and x_k .

3.4 Equations from boundary conditions

When the boundary condition of left end at the first span of continuous bridge is satisfied, it has Eq. (45)

$$\left. \begin{aligned} \phi_{b_1}(0) &= 0 \\ \phi''_{b_1}(0) &= 0 \end{aligned} \right\} \quad (45)$$

The substitution of Eq. (3) into Eq. (45), one obtains Eq. (46)

$$\left. \begin{aligned} B_{b_1} + D_{b_1} &= 0 \\ -B_{b_1} + D_{b_1} &= 0 \end{aligned} \right\} \quad (46)$$

or

$$\left[\mathbf{H}_{b_1} \right] \left\{ \mathbf{U}_{b_1} \right\} = 0 \quad (47)$$

where

$$\left[\mathbf{H}_{b_1} \right] = \begin{bmatrix} 1 & 2 & 3 & 4 \\ 0 & 1 & 0 & 1 \\ 0 & -1 & 0 & 1 \end{bmatrix} \quad (48)$$

$$\left\{ \mathbf{U}_{b_1} \right\} = \left\{ \begin{matrix} 1 & 2 & 3 & 4 \\ A_{b_1} & B_{b_1} & C_{b_1} & D_{b_1} \end{matrix} \right\}^T \quad (49)$$

$A_{b_1}, B_{b_1}, C_{b_1}$ and D_{b_1} are undetermined coefficients for modal shape function of section b_1 .

According to the right boundary condition, one obtains

$$\left. \begin{aligned} \phi_{b_{s+1}}(l_{b_{s+1}}) &= 0 \\ \phi_{b_{s+1}}''(l_{b_{s+1}}) &= 0 \end{aligned} \right\} \quad (50)$$

The substitution of Eq. (3) into Eq. (50), one obtains Eq. (51)

$$\left. \begin{aligned} A_{b_{s+1}} \sin \beta l_{b_{s+1}} + B_{b_{s+1}} \cos \beta l_{b_{s+1}} \\ + C_{b_{s+1}} \sinh \beta l_{b_{s+1}} + D_{b_{s+1}} \cosh \beta l_{b_{s+1}} &= 0 \\ l_{b_{s+1}} \beta^2 (-A_{b_{s+1}} \sin \beta l_{b_{s+1}} - B_{b_{s+1}} \cos \beta l_{b_{s+1}} \\ + C_{b_{s+1}} \sinh \beta l_{b_{s+1}} + D_{b_{s+1}} \cosh \beta l_{b_{s+1}}) &= 0 \end{aligned} \right\} \quad (51)$$

or

$$[\mathbf{H}_{b_{s+1}}] \{\mathbf{U}_{b_{s+1}}\} = 0 \quad (52)$$

where

$$[\mathbf{H}_{b_{s+1}}] = \begin{bmatrix} n''+1 & n''+2 & n''+3 & n''+4 \\ \sin \beta l_{b_{s+1}} & \cos \beta l_{b_{s+1}} & \sinh \beta l_{b_{s+1}} & \cosh \beta l_{b_{s+1}} \\ -\sin \beta l_{b_{s+1}} & -\cos \beta l_{b_{s+1}} & \sinh \beta l_{b_{s+1}} & \cosh \beta l_{b_{s+1}} \end{bmatrix} \begin{matrix} m''+1 \\ m''+2 \end{matrix} \quad (53)$$

$A_{b_{s+1}}, B_{b_{s+1}}, C_{b_{s+1}}$ and $D_{b_{s+1}}$ are undetermined coefficients for modal shape function of section b_{s+1} .

$$\{\mathbf{U}_{b_{s+1}}\} = \begin{bmatrix} A_{b_{s+1}} & B_{b_{s+1}} & C_{b_{s+1}} & D_{b_{s+1}} \end{bmatrix}^T \quad (54)$$

and

$$\left. \begin{aligned} m'' &= 12s + 4(j-2) + 2 \\ n'' &= 4(2s + (j-2)) + 4s \end{aligned} \right\} \quad (55)$$

4. Determination of natural frequencies and modal shapes

Continuous bridge shown in Fig. 1 is divided into $\{(2s+1)+(j-2)\}$ sections. At each section, there are four undetermined coefficients for modal shape function, and four undetermined coefficients for vehicle. Therefore, the whole number of undetermined coefficients for this system is $4\{(2s+1)+(j-2)\}+4s=12s+4j-4$. For each intermediate support, there are four undetermined coefficient equations (listed in Eq. (41)), four equations at two wheels of each vehicle (listed in Eqs. (12) and (21)), four equations for each vehicle (listed in Eq. (29)), two equations for boundary conditions at left and right supports. Therefore, the whole undetermined coefficients equations are $4(j-2)+4s \times 2+4s+4=12s+4j-4$. According to Eqs. (13)-(14), (22)-(23), (30)-(32), (42), (48) and (53), all elements in undetermined coefficient equations are given the identification number which are marked on the upper part and the right part of the matrices. Therefore, numerical assembly method is adopted to obtain the matrix equation of all undetermined coefficients, one has Eq. (56)

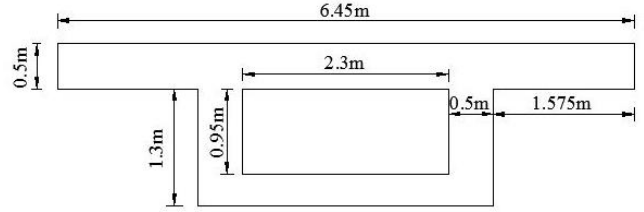


Fig. 2 Cross section for continuous bridge

$$[\mathbf{H}]\{\mathbf{U}\} = 0 \quad (56)$$

When the r th intermediate support is between the left and right wheels of p th vehicle ($x_1^p \leq x_r \leq x_2^p$), Elements identification numbers will change in undetermined coefficients equation matrices for wheels of p th vehicle, p th vehicle body and r th intermediate support (Appendix A). However, other identification numbers will not change.

Non-trivial solution of Eq. (56) requires that Eq. (57)

$$|\mathbf{H}| = 0 \quad (57)$$

The half-interval method (Lin and Tsai 2007) is used to determine the natural frequencies ω_i ($i=1,2,\dots$) of continuous bridge under multiple vehicles. For each order natural frequency, it satisfies Eq. (57). Mode shapes can be obtained by substituting natural frequencies ω_i ($i=1,2,\dots$) into Eq. (3). The accurate values of ω is obtained respectively using the half-interval method. The substitution of the obtained frequency ω into Eq. (3) will determine the corresponding mode shape of the beam.

5. Numerical simulation

5.1 Parameters for bridge

In this paper, uniform section is adopted (shown in Fig. 2) for continuous bridge. Elastic modulus for concrete is 2.85×10^{10} Pa, density is 2500 kg/m^3 .

5.2 Numerical results

5.2.1 Reliability of the proposed method

For vehicle model, wheel mass $m_{r1}=m_{r2}=1500 \text{ kg}$, sprung mass $m_b=1.77 \times 10^4 \text{ kg}$, rotatory mass $I_b=1.47 \times 10^5 \text{ kg} \cdot \text{m}^2$, suspension spring constant $k_{r1}=k_{r2}=2.4 \times 10^7 \text{ N/m}$, tyre stiffness parameters $k_{a1}=k_{a2}=2.4 \times 10^7 \text{ N/m}$, distance between wheels $a=4 \text{ m}$, and $s_1=s_2=0.5$.

The first three natural frequencies were calculated for two cases (shown in Fig. 3) by the proposed method in this paper. In order to verify the reliability of the method, finite element analysis (FEA) was also used to calculate the natural frequencies. The results were listed in Table 1.

For finite element model, the beam is divided into 80 beam elements with length 0.5 m and each element has two nodes, in which each node has rotational and vertical displacements. The mass matrix \mathbf{M} and stiffness matrix \mathbf{K} of beam elements are formed using Lagrange interpolation function, and equation of vibration is derived as follows

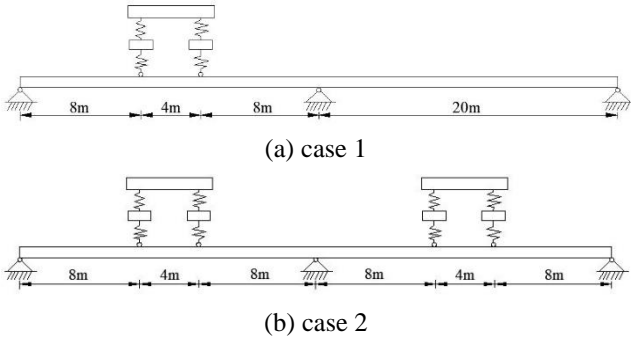


Fig. 3 Cases for reliability analysis of proposed method

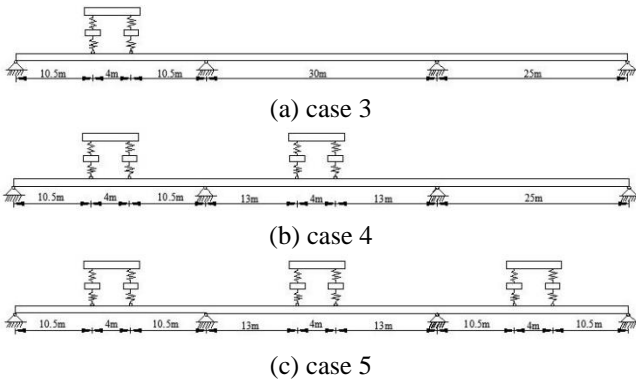


Fig. 4 Three cases for continuous bridge with three spans

$$\mathbf{M}_b \ddot{\mathbf{q}} + \mathbf{K}_b \mathbf{q} = \mathbf{\Phi}^T \mathbf{F}_b \quad (58)$$

where $\mathbf{M}_b = \mathbf{\Phi}^T \mathbf{M} \mathbf{\Phi}$, $\mathbf{K}_b = \mathbf{\Phi}^T \mathbf{K} \mathbf{\Phi}$, $\ddot{\mathbf{q}}$ is the 2nd order derivation of modal coordinates for beam, $\mathbf{\Phi}$ is the first n th order mode shape matrix of free vibration for beam, \mathbf{F}_b is the beam-vehicle interaction force.

$$\mathbf{F}_b = \mathbf{H} \begin{Bmatrix} P_1 \\ P_2 \end{Bmatrix} \quad (59)$$

here, \mathbf{H} is the location matrix of external force point; P_1 and P_2 are the forces of front and back wheel on the beam, respectively.

Eq. (59) is substituted into Eq. (58). Equation of beam-vehicle system can be obtained combining with Eqs. (4)-(5), which is shown as follows (Law and Zhu 2004)

$$\begin{bmatrix} \mathbf{M}_b & 0 \\ 0 & \mathbf{M}_v \end{bmatrix} \begin{Bmatrix} \ddot{\mathbf{q}} \\ \ddot{\mathbf{u}}_b \end{Bmatrix} + \begin{bmatrix} \mathbf{K}_b & \mathbf{K}_{bv} \\ \mathbf{K}_{bv}^T & \mathbf{K}_v \end{bmatrix} \begin{Bmatrix} \mathbf{q} \\ \mathbf{u}_b \end{Bmatrix} = 0 \quad (60)$$

where \mathbf{M}_v and \mathbf{K}_v are the mass and stiffness matrices of vehicle, respectively. \mathbf{K}_{bv} is coupling stiffness matrix of the beam-vehicle interaction system. Based on the finite element program constructed using MATLAB, modal properties of beam-vehicle system can be obtained by solving Eq. (58).

As can be seen from the results, natural frequencies calculated by the proposed method are consistent with the results of FEA. It reveals that the last solutions of proposed method are the exact ones. The reasons lie in that only the

Table 1 First three natural frequencies for two span uniform continuous bridge

Case No.	Methods	Natural frequencies		
		ω_1	ω_2	ω_3
Case 1	FEA (rad/s)	50.8395	77.5375	197.2940
	Present (rad/s)	50.8508	77.5350	197.4609
	Relative error (%)	0.022	0.003	0.085
Case 2	FEA (rad/s)	52.4060	78.1533	197.8355
	Present (rad/s)	52.3906	78.1592	198.0078
	Relative error (%)	0.029	0.008	0.087

Table 2 First three natural frequencies for three span uniform continuous bridge

Cases	Natural frequencies (rad/s)		
	ω_1	ω_2	ω_3
No vehicles	26.77	39.24	49.36
Case 3	26.24	42.06	50.43
Case 4	25.66	42.38	51.42
Case 5	25.33	44.26	52.10

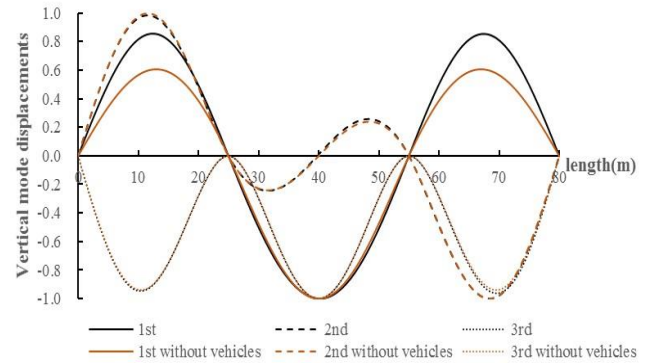


Fig. 5 Modal shapes for case 3

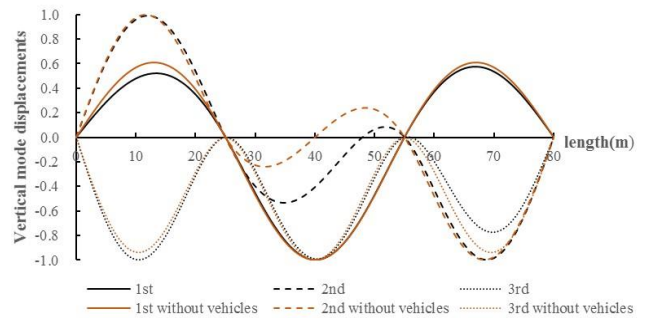


Fig. 6 Modal shapes for case 4

differential equations of motion for continuous bridge and vehicles were used to make the undetermined coefficients equations, and no other assumptions were introduced.

5.2.2 Natural frequencies and modal shapes for continuous bridge under multiple vehicles

The same vehicle parameters were adopted as listed in section 5.2.1. Three different cases were established and shown in Fig. 4. The first three natural frequencies and corresponding modal shapes were calculated for these three

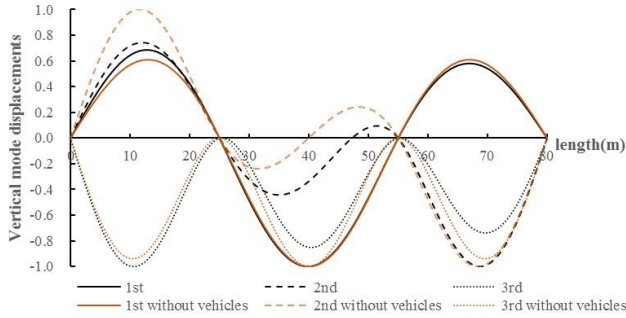


Fig. 7 Modal shapes for case 5

Table 3 Four different vehicle parameters

Vehicle parameters	m_{r1}, m_{r2} ($m_{r1}=m_{r2}$) (kg)	m_b (kg)	I_b ($\text{kg} \cdot \text{m}^2$)	k_{r1}, k_{r2} ($k_{r1}=k_{r2}$) (N/m)	k_{a1}, k_{a2} ($k_{a1}=k_{a2}$) (N/m)	a (m)	s_1, s_2 ($s_1=s_2$)
Vehicle 1	1500	1.77×10^4	1.47×10^5	2.4×10^7	2.4×10^7	4	0.5
Vehicle 2	1500	1.77×10^4	1.47×10^5	3.55×10^7	3.55×10^7	4	0.5
Vehicle 3	1500	1.77×10^4	1.47×10^5	1×10^9	1×10^9	4	0.5
Vehicle 4	1500	1.77×10^4	1.47×10^5	1×10^8	1×10^8	4	0.5

Table 4 First four natural frequencies of vehicle model

Vehicle parameters	ω_{vv}^1 (rad/s)	ω_{vv}^2 (rad/s)	ω_{vv}^3 (rad/s)	ω_{vv}^4 (rad/s)
Vehicle 1	23.75	29.03	180.52	181.33
Vehicle 2	28.90	35.31	219.53	220.54
Vehicle 3	304.23	413.12	1200.3	1250.1
Vehicle 4	96.20	130.63	379.57	395.34

cases and continuous bridge without vehicles. Natural frequencies were listed in Table 2, while modal shapes were shown in Figs. 5-7.

As can be seen from the results, the first natural frequencies of continuous bridge under different number of vehicles (cases 3-5) are lower than those without vehicles. However, the second and third natural frequencies for cases 3, 4 and 5 are higher than those without vehicles. Differences of natural frequencies caused by vehicles are related to the vehicle quantity. The more the number of vehicles are, the greater the influence on natural frequencies. As for modal shapes, there are some differences when vehicle effects are considered or not. Moreover, the differences are dependent on vehicle positions and numbers.

5.2.3 Influence of vehicle parameters on natural frequencies

Different vehicle parameters were determined and listed in Table 3. For these vehicles, each has four freedoms. Therefore, four natural frequencies (ω_{vv}^1 , ω_{vv}^2 , ω_{vv}^3 and ω_{vv}^4) can be calculated for each vehicle model. Calculation results of natural frequencies for vehicles were listed in Table 4.

One vehicle was carried by a two span continuous bridge (shown in Fig. 8). Left wheel of vehicle is located at different positions statically and its change direction is from A to B, corresponding first order of natural frequencies

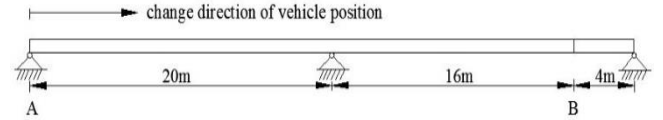


Fig. 8 Schematic diagram for the change direction of vehicle position (left wheel) statically

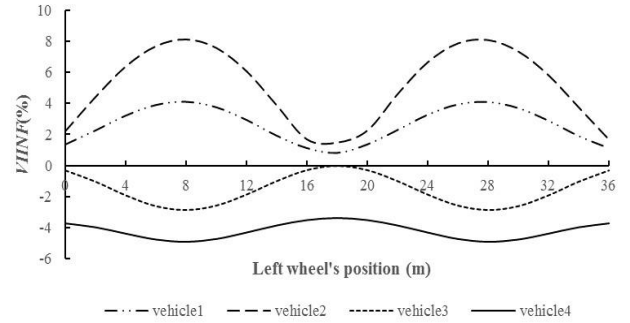


Fig. 9 Relation curve between VIINF and action position of left wheel

were calculated by the proposed method. In order to evaluate the influence of vehicle parameters on natural frequencies, following index was defined and calculated by

$$VIINF = \frac{\omega_v^1 - \omega_0^1}{\omega_0^1} \times 100\% \quad (61)$$

where $VIINF$ is vehicle influence index on natural frequency; ω_0^1 is the first natural frequency of bridge without vehicle; while ω_v^1 is the first natural frequency of bridge under the effect of vehicle.

Relationships between $VIINF$ and left wheel positions of vehicles are shown in Fig. 9.

As can be seen from Fig. 9, the amplitude effect is more obvious when the left wheel is acting on the mid-span of bridge. The first order natural frequencies of continuous bridge under the vehicle are higher than that without vehicle when parameters of vehicles 1 and 2 are adopted. However, they are lower when parameters of vehicles 3 and 4 are used. The first natural frequency ω_0^1 for continuous bridge without vehicle is 48.83rad/s, which is between the second order frequency (ω_{vv}^2) and the third order frequency (ω_{vv}^3) for vehicle 1 and vehicle 2 (as listed in Table 4). However, ω_0^1 is lower than ω_{vv}^1 ($\omega_{vv}^1 > \omega_0^1$) for vehicle 3 and vehicle 4. Therefore, one conclusion can be obtained for assessing relative size of ω_0^1 and ω_v^1 based on above research results. That is the closest vehicle frequency (ω_{vv}^i) to natural frequency of bridge without vehicle (ω_0^1) should be determined firstly. Then, ω_{vv}^i and ω_0^1 are compared. If $\omega_{vv}^i > \omega_0^1$, $\omega_v^1 < \omega_0^1$; if $\omega_{vv}^i < \omega_0^1$, $\omega_v^1 > \omega_0^1$. Other cases are also simulated and used to verify above result and that is applicable. This conclusion is also consistent with the research result by Law and Zhu (2004) and this method has more extensive applicability.

6. Conclusions

In this paper, free vibration analysis of continuous bridge under multiple vehicles is presented. The exact solutions for natural frequencies and mode shapes of bridge considering bridge-vehicle interactions are obtained based on numerical assembly method. Numerical simulation on continuous bridge with uniform box section is used to verify its feasibility. Comparative analysis with FEA results indicates that the proposed method possesses favorable accuracy, which can be regarded as exact solution. Natural frequencies and modal shapes of continuous bridge with different conditions (number and position) of vehicles are also investigated and compared with bridge without vehicles. It reveals that differences of natural frequencies and modal shapes caused by vehicles are highly related to vehicle position and numbers. Finally, the influence of vehicle parameters on the first order natural frequency is discussed, and totally four different groups of vehicle parameters were used. It can be concluded that the first order natural frequencies of bridge under effect of vehicles are closely associated with vehicles parameters. Corresponding judgment method is also proposed.

Acknowledgments

The authors express their appreciation for financial supports of National Natural Science Foundation of China under Grants nos. 51478203 and 51408258; China Postdoctoral Science Foundation funded project (nos. 2014M560237 and 2015T80305); Fundamental Research Funds for the Central Universities and Science (JCKYQKJC06), and Technology Development Program of Jilin Province.

References

- Ahmari, S., Yang, M. and Zhong, H. (2015), "Dynamic interaction between vehicle and bridge deck subjected to support settlement", *Eng. Struct.*, **84**, 172-183.
- Azimi, H., Galal, K. and Pekau, O.A. (2013), "A numerical element for vehicle-bridge interaction analysis of vehicles experiencing sudden deceleration", *Engi. Struct.*, **49**(2), 792-805.
- Biggs, J.M. and Suer, H.S. (1956), "Vibration measurements on simple-span bridges", *Highw. Res. Board Bull.*, **124**, 1-15.
- Cha, P.D. (2001), "Natural frequencies of a linear elastica carrying any number of sprung masses", *J. Sound Vib.*, **247**(1), 185-194.
- Gao, Q., Wang, Z., Ghee Koh, C. and Chen, C. (2015), "Dynamic load allowances corresponding to different responses in various sections of highway bridges to moving vehicular loads", *Adv. Struct. Eng.*, **18**(10), 1685-1702.
- Karimi, A.H. and Ziaei-Rad, S. (2015), "Nonlinear coupled longitudinal-transverse vibration analysis of a beam subjected to a moving mass traveling with variable speed", *Arch. Appl. Mech.*, **85**(12), 1941-1960.
- Kim, C.W., Kawatani, M. and Kim, K.B. (2005), "Three-dimensional dynamic analysis for bridge-vehicle interaction with roadway roughness", *Comput. Struct.*, **83**(19), 1627-1645.
- Kim, C.Y., Jung, D.S., Kim, N.S., Kwon, S.D. and Feng, M.Q. (2003), "Effect of vehicle weight on natural frequencies of bridges measured from traffic-induced vibration", *Earthq. Eng. Eng. Vib.*, **2**(1), 109-115.
- Kumar, C.S., Sujatha, C. and Shankar, K. (2015), "Vibration of simply supported beams under a single moving load: A detailed study of cancellation phenomenon", *Int. J. Mech. Sci.*, **99**, 40-47.
- Law, S.S. and Zhu, X.Q. (2004), "Dynamic behavior of damaged concrete bridge structures under moving vehicular loads", *Eng. Struct.*, **26**(9), 1279-1293.
- Lin, H.Y. and Tsai, Y.C. (2007), "Free vibration analysis of a uniform multi-span beam carrying multiple spring-mass systems", *J. Sound Vib.*, **302**(3), 442-456.
- Liu, J.B. and Du, X.L. (2005), *Dynamics of Structures*, China Machine Press, Beijing, China.
- Naguleswaran, S. (2003), "Transverse vibration of an Euler-Bernoulli uniform beam on up to five resilient supports including ends", *J. Sound Vib.*, **261**, 372-384.
- O'Brien, E., Carey, C. and Keenahan, J. (2015), "Bridge damage detection using ambient traffic and moving force identification", *Struct. Control Health Monit.*, **22**, 1396-1407.
- Rieker, J.R. and Trethewey, M.W. (1999), "Finite element analysis of an elastic beam structure subjected to a moving distributed mass train", *Mech. Syst. Signal Pr.*, **13**(1), 31-51.
- Shi, L.N., Yan, W.M. and He, H.X. (2014), "The modal characteristics of non-uniform multi-span continuous beam bridges", *Struct. Eng. Mech.*, **52**(5), 997-1017.
- Shirai, H. (2008), "Development of a numerical model for bridge-vehicle interaction and human response to traffic-induced vibration", *Eng. Struct.*, **30**(12), 3808-3819.
- Stokes, G.G. (1849), "Discussion of a differential equation relating to the breaking of railway bridges", *Transactions of the Cambridge Philosophical Society*, Part 5, 707-735.
- Tan, G.J., Gong, Y.F., Cheng, Y.C., Liu, H.B. and Wang, L.L. (2011), "Calculation for natural frequency of simply supported beam bridges based on loaded frequency", *J. Vib. Eng.*, **24**(1), 31-35. (in Chinese)
- Wang, J. and Qiao, P. (2007), "Vibration of beams with arbitrary discontinuities and boundary conditions", *J. Sound Vib.*, **308**, 12-27.
- Willis, R. (1849), *Commissioners report: application of iron to railway structures*, William Clowes & Sons, London.
- Wu, J.S. and Chou, H.M. (1999), "A new approach for determining the natural frequencies and mode shapes of a uniform beam carrying any number of sprung masses", *J. Sound Vib.*, **220**(3), 451-468.
- Yang, Y.B. and Lin, C.W. (2005), "Vehicle-bridge interaction dynamics and potential applications", *J. Sound Vib.*, **284**(1), 205-226.
- Yang, Y.B. and Yau, J.D. (1997), "Vehicle-bridge interaction element for dynamic analysis", *J. Struct. Eng.*, **123** (11), 1512-1518.
- Yin, X.F., Fang, Z., Cai, C.S. and Deng, L. (2010), "Non-stationary random vibration of bridges under vehicles with variable speed", *Eng. Struct.*, **32**, 2166-2174.
- Zhu, X.Q. and Law, S.S. (2002), "Dynamic load on continuous multi-lane bridge deck from moving vehicles", *J. Sound Vib.*, **251**(4), 697-716.

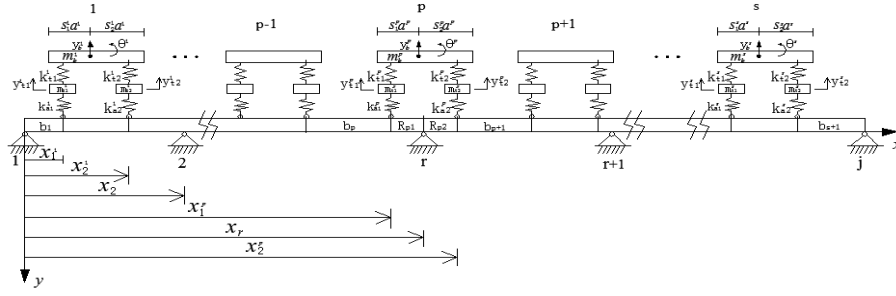


Fig. A-1 Vehicle distribution when $x_1^p \leq x_r \leq x_2^p$

Appendix A

If the r th intermediate support is between left wheel and right wheel of p th vehicle ($x_1^p \leq x_r \leq x_2^p$), corresponding vehicle distribution is shown in Fig. A-1.

Section b_{R_p} in Fig. 1 is replaced by $b_{R_{p1}}$ in Fig. A-1, Eq. (12) can be expressed by Eq. (a1)

$$[\mathbf{H}_{pl}]\{\mathbf{U}_{pl}\} = \left[\begin{array}{cccc} \mathbf{H}_{pl_1} & \mathbf{H}_{pl_2} & 0 & \mathbf{H}_{pl_3} \end{array} \right] \left\{ \begin{array}{l} \mathbf{U}_{b_p} \\ \mathbf{U}_{R_{p1}} \\ \mathbf{U}_{R_{p2}} \\ \mathbf{U}_{pv} \end{array} \right\} \quad (\text{a1})$$

$$[\mathbf{H}_{pl}] = \left[\begin{array}{cccc} & & & 0 \\ & \mathbf{H}_{pl_1} & \mathbf{H}_{pl_2} & 0 \\ & & & 0 \\ & & & 0 \end{array} \right] \quad (\text{a2})$$

$$\left[\begin{array}{cccc} n+10 & n+11 & n+12 & n+13 \rightarrow n+16 \\ 0 & 0 & 0 & \\ 0 & 0 & 0 & \mathbf{H}_{pl_3} \\ 0 & 0 & 0 & \\ 0 & 0 & 0 & \end{array} \right] \left\{ \begin{array}{l} m+1 \\ \downarrow \\ m+4 \end{array} \right.$$

$$\{\mathbf{U}_{pl}\} = \left\{ \begin{array}{cc} n+1 \rightarrow n+4 & n+5 \rightarrow n+8 \\ \mathbf{U}_{b_p} & \mathbf{U}_{R_{p1}} \\ n+9 \rightarrow n+12 & n+13 \rightarrow n+16 \\ \mathbf{U}_{R_{p2}} & \mathbf{U}_{pv} \end{array} \right\}^T \quad (\text{a3})$$

l_{R_p} in Eq. (12) is replaced by $l_{R_{p1}}$, one obtains Eqs. (a2)-(a4)

$$\left. \begin{array}{l} m = 12(p-1) + 4(r-2) + 2 \\ n = 4\{2(p-1) + (r-2)\} \\ + 4(p-1) = 12(p-1) + 4(r-2) \end{array} \right\} \quad (\text{a4})$$

Section R_p in Fig. 1 is replaced by R_{p2} in Fig. (A-1), Eq. (21) can be expressed by Eq. (a5)

$$[\mathbf{H}_{pr}]\{\mathbf{U}_{pr}\} = \left[\begin{array}{cccc} 0 & \mathbf{H}_{pr_1} & \mathbf{H}_{pr_2} & \mathbf{H}_{pr_3} \end{array} \right] \left\{ \begin{array}{l} \mathbf{U}_{R_{p1}} \\ \mathbf{U}_{R_{p2}} \\ \mathbf{U}_{pv} \\ \mathbf{U}_{b_{p+1}} \end{array} \right\} \quad (\text{a5})$$

l_{R_p} in Eq. (21) is replaced by $l_{R_{p2}}$, one obtains Eqs. (a6)-(a7)

$$[\mathbf{H}_{pr}] = \left[\begin{array}{cccccc} n+5 & n+6 & n+7 & n+8 & n+9 \rightarrow n+12 & \\ 0 & 0 & 0 & 0 & & \mathbf{H}_{pr_1} \\ 0 & 0 & 0 & 0 & & \\ 0 & 0 & 0 & 0 & & \\ 0 & 0 & 0 & 0 & & \end{array} \right] \quad (\text{a6})$$

$$\left. \begin{array}{cc} n+13 \rightarrow n+16 & n+17 \rightarrow n+20 \\ \mathbf{H}_{pr_2} & \mathbf{H}_{pr_3} \end{array} \right\} \left\{ \begin{array}{l} m+5 \\ \downarrow \\ m+8 \end{array} \right.$$

$$\{\mathbf{U}_{pr}\} = \left\{ \begin{array}{cc} n+5 \rightarrow n+8 & n+9 \rightarrow n+12 \\ \mathbf{U}_{R_{p1}} & \mathbf{U}_{R_{p2}} \\ n+13 \rightarrow n+16 & n+17 \rightarrow n+20 \\ \mathbf{U}_{pv} & \mathbf{U}_{b_{p+1}} \end{array} \right\}^T \quad (\text{a7})$$

Eq. (29) can be changed into Eqs. (a8)-(a9)

$$[\mathbf{H}_v^p]\{\mathbf{U}_v^p\} = \left[\begin{array}{cccc} \mathbf{H}_{v_1}^p & 0 & \mathbf{H}_{v_2}^p & \mathbf{H}_{v_3}^p \end{array} \right] \left\{ \begin{array}{l} \mathbf{U}_{R_{p1}} \\ \mathbf{U}_{R_{p2}} \\ \mathbf{U}_{pv} \\ \mathbf{U}_{b_{p+1}} \end{array} \right\} \quad (\text{a8})$$

$$[\mathbf{H}_v^p] = \left[\begin{array}{cccc} n+5 \rightarrow n+8 & n+9 & n+10 & n+11 \\ & 0 & 0 & 0 \\ \mathbf{H}_{v_1}^p & 0 & 0 & 0 \\ & 0 & 0 & 0 \\ & 0 & 0 & 0 \end{array} \right] \quad (\text{a9})$$

Sections b_{q+1} and b_{k+1} in Fig. 1 are replaced by R_{p1} and R_{p2} , respectively; $l_{b_{q+1}}$, $l_{b_{k+1}}$ in Eq. (39) is replaced by

$l_{R_{p1}}$ and $l_{R_{p2}}$, respectively. Then, Eqs. (40)-(41) can be transformed into Eqs. (a10)-(a11)

$$\begin{aligned}
 & \begin{matrix} n+5 & n+6 & n+7 \\ \left[\mathbf{H}_s \right] = & \begin{bmatrix} \sin \beta l_{R_{p1}} & \cos \beta l_{R_{p1}} & \sinh \beta l_{R_{p1}} \\ 0 & 0 & 0 \\ \cos \beta l_{R_{p1}} & -\sin \beta l_{R_{p1}} & \cosh \beta l_{R_{p1}} \\ -\sin \beta l_{R_{p1}} & -\cos \beta l_{R_{p1}} & \sinh \beta l_{R_{p1}} \end{bmatrix} \\ & \begin{matrix} n+8 & n+9 & n+10 & n+11 & n+12 \end{matrix} \end{matrix} \quad (a10) \\
 & \begin{matrix} \cosh \beta l_{R_{p1}} & 0 & 0 & 0 & 0 \\ 0 & 0 & 1 & 0 & 1 \\ \sinh \beta l_{R_{p1}} & -1 & 0 & -1 & 0 \\ \cosh \beta l_{R_{p1}} & 0 & 1 & 0 & -1 \end{matrix} \left. \begin{matrix} \\ \\ \\ \\ \end{matrix} \right\} \begin{matrix} m+13 \\ m+14 \\ m+15 \\ m+16 \end{matrix}
 \end{aligned}$$

$$\begin{aligned}
 & \begin{matrix} n+5 \rightarrow n+8 & n+9 \rightarrow n+12 \\ \left\{ \mathbf{U}_s \right\} = \left\{ \begin{matrix} \mathbf{U}_{R_{p1}} & \mathbf{U}_{R_{p2}} \end{matrix} \right\}^T \end{matrix} \quad (a11)
 \end{aligned}$$